Acta Geochim (2025) 44:844–857
https://doi.org/10.1007/s11631-025-00791-w

ORIGINAL ARTICLE

Prolonged mantle metasomatism in the Neoproterozoic continental arc: Insights from mafic magmatism in the western Yangtze Block, South China

Zhe-hao Zhong[1] · Shao-cong Lai[1] · Yu Zhu[2,3] · Jiang-feng Qin[1] · Ren-zhi Zhu[1] · Min Liu[1] · Yu-hong Xia[1]

Received: 15 January 2025 / Revised: 25 April 2025 / Accepted: 20 May 2025 / Published online: 23 June 2025

Abstract Mafic rocks generated from subduction settings have recorded valuable source information about the mantle source. In this study, we present a comprehensive analysis of zircon U–Pb dating, whole-rock major and trace elements, and Sr–Nd isotopic data for the mafic gabbro located in the Yumen area, on the western part of the Yangtze Block, South China, aiming to constrain the processes of mantle metasomatism within subduction settings. U–Pb dating results for zircon yield crystallization ages of 800 Ma for type 1 mafic gabbro and 753–734 Ma for type 2 mafic gabbro. Type 1 mafic gabbro exhibits higher SiO_2 (44.13%–48.93%) and Al_2O_3 content but lower total Fe_2O_3 and MgO content than type 2 gabbro (SiO_2: 41.02%–43.28%). These gabbros display a high-$Mg^{\#}$ signature (52.50–62.81 for type 1, 50.89–57.04 for type 2), while they are enriched in significant large-ion lithophile elements (LILEs: Rb, Ba, Sr, K) and depleted in high-field-strength elements (HFSEs: Zr, Hf, Nd, Ta, Ti), which indicates an arc-like element signature. The positive whole-rock εNd(t) values (type 1: 3.5–4.4, type 2: 5.6–6.3) combined with a narrow range of $(^{87}Sr/^{86}Sr)_i$ (type 1: 0.7035–0.7043, type 2: 0.7035–0.7036) of both gabbro types suggest a depleted lithospheric mantle origin. Therefore, these mafic rocks may derive from a metasomatized spinel lherzolite mantle source (with amphibole) due to the interactions of the deep mantle source and subduction fluid materials. We propose that the long-term metasomatism recorded by mafic gabbro in this study supports the fact that the subduction during the Neoproterozoic contributed to the formation of a metasomatized mantle source in the Yumen area, western Yangtze Block, South China.

Keywords Mafic rocks · Mantle Metasomatism · Subbduction

1 Introduction

Mafic magmatism derived from the subduction zone provides valuable insights for exploring the heterogeneous mantle source. Specific mafic rocks can effectively constrain the

Supplementary Information The online version contains supplementary material available at https://doi.org/10.1007/s11631-025-00791-w.

✉ Shao-cong Lai
shaocong@nwu.edu.cn

✉ Yu Zhu
yuzhunwu@163.com

Zhe-hao Zhong
Zhongzhnwu@163.com

Jiang-feng Qin
qinjf@nwu.edu.cn

Ren-zhi Zhu
renzhi@nwu.edu.cn

Min Liu
liumin@nwu.edu.cn

Yu-hong Xia
xiayhgeo@163.com

[1] State Key Laboratory of Continental Dynamics, Department of Geology, Northwest University, Xi'an 710069, China

[2] Hubei Key Laboratory of Petroleum Geochemistry and Environment, College of Resources and Environment, Yangtze University, Wuhan 430100, China

[3] YU CUGW Joint Research Center on Deep Earth and Surface Dynamic Coupling, College of Resources and Environment, Yangtze University, Wuhan 430100, China

heterogeneous source property (e.g., source composition) through bulk geochemistry (Tatsumi 1989; Wilson 1989; Zheng et al. 2020). The intricate processes of mafic magma from formation to emplacement recorded both source property and metasomatism modification (Davidson 1987; Plank and Langmuir 1998; Wilson 1989). Thus, mafic rocks in subduction-related settings provide an ideal research object to better understand the metasomatism processes due to interactions between the deep mantle source and the subduction slab. Subduction-derived components (e.g., sediments and fluids) can be introduced into variable depths beneath the subduction zone to generate a diversity of subduction-related mafic rocks (Barry et al. 2006; Grove et al. 2002; Peacock 1990). Thus, subduction-related ultramafic–mafic rocks derived from the mantle may survive variable degrees of modification by subduction-related components (e.g., slab-melt, slab-fluid, slab-sediment), which certainly alter the magma source composition and state (Wilson 1989).

During the Neoproterozoic, complicated geological processes formed numerous ultramafic–mafic rocks, in particular along the western area of the Yangtze Block, South China. These diverse rock types (e.g., gabbro, picrite, dolerite) provide a good opportunity to enhance our understanding of the crust–mantle mixing dynamic process and subsequent metasomatism modification of the magma source (Du et al. 2014; Li et al. 2003; Munteanu et al. 2010; Sun and Zhou 2008; Yang et al. 2017; Zhao and Zhou 2007; Zhao et al. 2019; Zhou et al. 2006; Zhu et al. 2008, 2019, 2021) (Fig. 1c).

This paper presents whole-rock data in a combination of trace element and Sr–Nd isotope analytical results via investigation of the petrogenesis and geodynamic processes of the mafic gabbro newly discovered in the Yumen area, South China, to further our understanding of the interactions and geodynamic significance during subduction processes. The two types of mafic gabbro indicate long-term magmatism with subduction-related fluid metasomatism and an amphibole-bearing mantle source. This study aims to reveal the long-lived metasomatism modification of the mantle source under a subduction setting beneath the western margin of the Yangtze Block.

2 Geological background and sample petrography

The South China Block in eastern Asia primarily comprises the Yangtze Block in the west and the Cathaysia Block in the east. These sub-blocks were welded during the Mesoproterozoic to Neoproterozoic time, and two blocks were separated by the Jiangnan orogen as its boundary (Zhao and Cawood 2012; Zheng et al. 2013). The Yangtze Block is tectonically bounded by the Qinling-Dabie Orogenic Belt and Longmenshan Overthrust Belt to the north, and the Ailaoshan Song Ma Fault and Jiangnan Orogen to the South (Zhao and Cawood 2012; Zhao et al. 2018; Zhou et al. 2006) (Fig. 1a, b). The western boundary is delimited by the Tibetan Plateau (Fig. 1a). The Yangtze Block consists of Archean to Paleoproterozoic crystalline basement (e.g., Kongling complex) overlain by Mesoproterozoic–Neoproterozoic low-degree

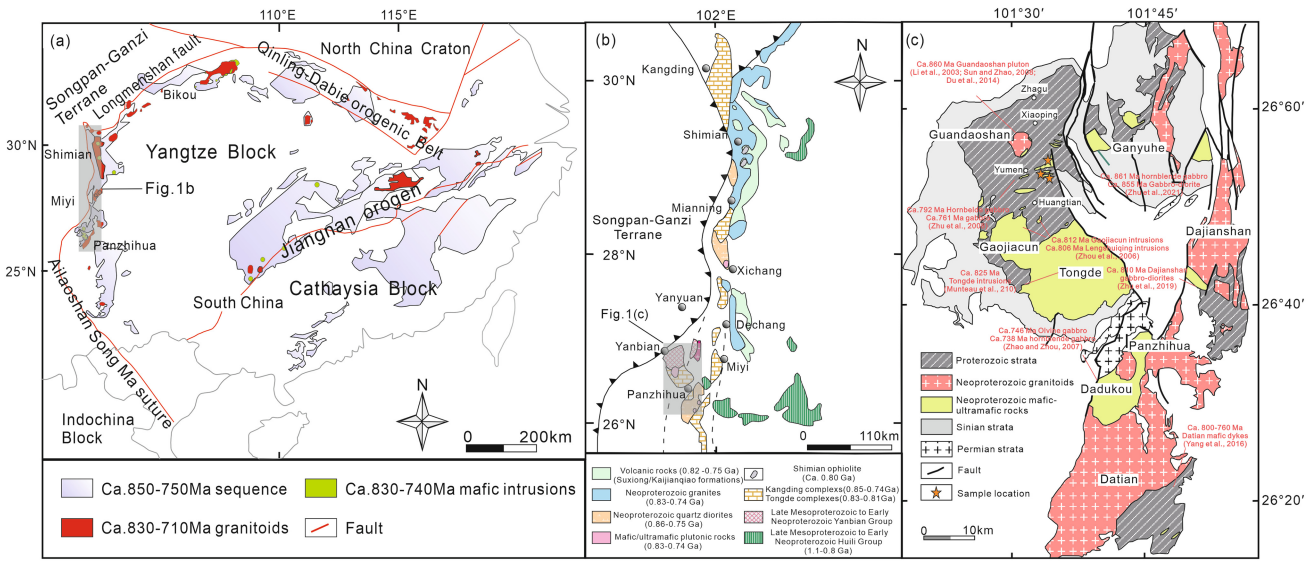

Fig. 1 Simplified geological map of the Yangtze Block, South China (**a**, **b**) (modified after Zhao and Cawood 2012 and Zhao et al. 2018) and regional geological map of the studied granites in the Yonglang area along the western Yangtze Block, South China (**c**) (modified after Miyi 1:200,000 geological map, SPBGMR 1972; Zhu et al. 2016). The Neoproterozoic mafic dyke/intrusion/pluton locations are highlighted with grass green labels in (**c**) (Du et al. 2014; Li et al. 2003; Munteanu et al. 2010; Sun and Zhou 2008; Yang et al. 2017; Zhao and Zhou 2007; Zhao et al. 2019; Zhou et al. 2006; Zhu et al. 2008; Zhu et al. 2019; Zhu et al.2021)

metamorphosed strata (e.g., Banxi Group) and late Neoproterozoic Sinian unmetamorphosed sediment sequences (Li et al. 2006; Zhao and Cawood 2012). The Mesoproterozoic strata are mainly distributed in the southwestern part, while the Archean Kongling and Huangtuling complexes crop out in the northern–northeastern region of the Yangtze Block. The southwestern margin of the Yangtze Block displays volcanic–sedimentary sequences that date back to the Meso-Neoproterozoic periods. Among these sequences are notable late Mesoproterozoic formations, including the Kunyang and Huili Groups, only distributed along the southwestern edge of the Yangtze Block (Greentree et al. 2006; Zhao et al. 2018; Zhao and Cawood 2012; Zhu et al. 2016). In the western edge of the Yangtze Block, Neoproterozoic Yanbian terrane consists of the Yanbian Group (2000-m-thick Fangtian formation, 2200-m-thick Xiaoping Formation, 1100-m-thick Zagu formation), a sedimentary–volcanic sequence of nearly 6000 m (mainly consisting of clastic rocks and lavas), which was intruded by numerous ultramafic–mafic plutons and overlain by Sinian strata (Du et al. 2014; Li et al. 2006; Zhou et al. 2006). During the Neoproterozoic period, numerous sedimentary–volcanic strata, felsic intrusive rocks, and widespread mafic–ultramafic intrusive rocks emerged (Zhao and Zhou 2007, 2009; Zhao et al. 2018), including the Guandaoshan (~860 Ma), Lengshuiqing (~840 Ma), Gaojiacun (~840 Ma), and Dadukou (~820 Ma) ultramafic–mafic rocks, mafic ultra mafic rocks arising and intruding to the Yanbian Group, and hornblende gabbro and olivine gabbro (~740 Ma) in the northeastern part of Panzihua near the Yanbian Group also dated during the Neoproterozoic, recording the prolonged magma events (Du et al. 2014; Meng et al. 2015; Zhao and Zhou 2007; Zhao et al. 2019; Zhou et al. 2006; Zhu et al. 2008, 2020). These plutons have zircon U–Pb ages dated at ca. 0.83–0.74 Ga, and the mafic–ultramafic intrusive rocks in particular have experienced long-term evolution and introduction of diverse subduction-related components, which provides new insight to evaluate the long-term magmatism beneath the western margin of the Yangtze Block (Du et al. 2014; Meng et al. 2015; Zhao and Zhou 2007; Zhao et al. 2019; Zhou et al. 2006; Zhu et al. 2008).

The mafic rock samples are collected from several Neoproterozoic mafic–ultramafic rocks, which dispersedly crop out near the Yumen area, in Yanbian terrane, southern part of the western Yangtze Block, South China (GPS position: YM-1, YM-2 26°56′24″N 101°35′16″E, YM-3 26°55′9″N 101°34′30″E, YM-4 26°51′15″N 101°31′2″E) (Fig. 1c). These mafic–ultramafic rocks closely contact the Proterozoic strata. Field geology shows that these mafic rocks intrude the country rock, mainly consisting of carbonaceous slate and tuffaceous slate. In contrast to weak metamorphism and deformation of wall rocks, the absence of metamorphism and deformation is observed in most mafic rocks (Fig. 2b).

The mafic gabbro samples obtained from the Yumen area exhibit a texture that ranges from gray to dark gray, characterized by medium to fine granularity (Fig. 2a, b). The mafic rocks were subdivided and classified into two distinct types based on the details of petrology research via microscopic observation and investigation during the field study.

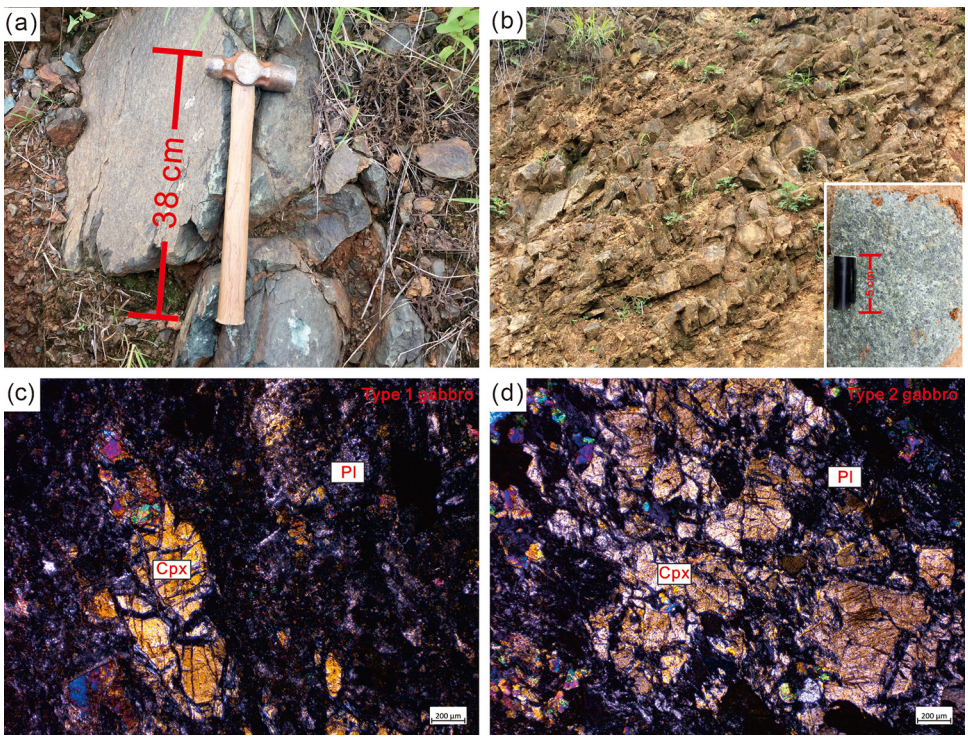

Fig. 2 The field images of Early Neoproterozoic mafic gabbro in this study (**a**, **b**) and microscope images of mafic gabbro via cross-polarized illumination of an optical microscope (**c**, **d**). The representative images of type 1 and type 2 gabbro are presented in **c** and **d**, respectively

The type 1 mafic gabbro (YM-4, YM-3) mainly consists of gabbro, composed of plagioclase (45%–60%) and clinopyroxene (40%–50%), with minor Fe–Ti oxide (Fig. 2c, d). In comparison, the type 2 mafic gabbro (YM-2, YM-1) displays similar mineral composition but is distinguished by higher clinopyroxene (50%–60%) content, lower plagioclase content (40%–50%), and increased concentrations of Fe–Ti oxides. Clinopyroxene exhibits euhedral to subhedral forms, with fragmentation occurring in the clinopyroxene margin. Plagioclases are generally coarse-grained and subhedral to anhedral, although many plagioclases have experienced variable degrees of post-magmatic alteration, such as epidotization and chloritization, while associated clinopyroxenes remain comparatively unaltered. The absence of amphiboles may be attributed to the processes of chloritization.

3 Analytical procedures

3.1 Zircon U–Pb analysis

Zircon grains were carefully separated from samples of YM-1, YM-2, and YM-3 through the heavy liquid/magnetic method, and then grains with representative features were selected under a binocular microscope. Representative zircon grains were mounted in epoxy resin discs and then polished to ensure that the carbon coating was on a flat surface. The cathodoluminescence (CL) microscopy and U–Pb isotopic analyses were carried out at the State Key Laboratory of Continental Dynamics, Northwest University, Xi'an, China, and the internal morphology of the zircons was obtained before the analyses of U–Pb isotopes. Based on the methodology outlined by Yuan et al. (2004), a 193-nm laser was set in an Agilent 7500a inductively coupled plasma mass spectroscopy (ICP-MS) unit to perform laser ablation–inductively coupled plasma mass spectrometry (LA-ICP-MS) U–Pb analyses. The GLITTER program was applied to calculate the $^{207}Pb/^{206}Pb$ and $^{206}Pb/^{238}U$ ratios, and the Havard zircon 91500 external calibration standard was used to correct the results (Wiedenbeck et al. 2004). Yuan et al. (2004) presented detailed analytical procedures and methodology. Methods described by Andersen (2002) were then conducted to calibrate the standard Pb concentrations. Using the Isoplot toolkit (version 3.0) developed by Ludwig (2003), concordia diagrams of the concordant age were drawn, and age was calculated simultaneously, with uncertainties expressed at the 1σ confidence level.

3.2 Whole-rock geochemistry and Sr–Nd isotopes

Fresh parts of samples were selected, the weathered surfaces were removed, and samples were mounted to a tungsten carbide ball mill; fresh samples were chipped and powdered to ~200 mesh. Powder samples were analyzed, with whole-rock major and trace elemental analyses conducted via X-ray fluorescence (XRF; Rigaku RIX 2100) at the State Key Laboratory of Continental Dynamics, Northwest University in Xi'an, and strontium–neodymium (Sr–Nd) isotopic analyses performed using ICP-MS (Agilent 7500a). Sample powders were digested using a mixture of hydrofluoric acid (HF) and nitric acid (HNO_3) in high-pressure Teflon bombs at 190 °C for 48 h. The analytical error was less than 2%, and the precision was greater than 10% (Liu et al. 2007). The national rock standards (BCR-2, GSR-1, and GSR-3) are applied to analyses in this study; analytical results indicate that both analytical precision and accuracy for the major elements are generally better than 5%.

Whole-rock Sr–Nd isotopic data were obtained using a Neptune Plasma II multi-collector mass spectrometer at Nanjing FocuMS Technology Co. Ltd. (Nanjing, China). During the sample runs, the NBS987 standard yielded an average value of $^{87}Sr/^{86}Sr = 0.710318 \pm 4$ (1σ). The BCR-1 standard and W-2 standard yielded average values of $^{87}Sr/^{86}Sr = 0.704980 \pm 3$ (1σ) and $^{87}Sr/^{86}Sr = 0.706895 \pm 3$ (1σ), respectively. The results for the standard material are reliable, with negligible deviation from reference values ($^{87}Sr/^{86}Sr$ reference value; NBS987 = 0.710340; BCR-1 = 0.705014 ± 33; W-2 = 0.706965 ± 4; 1σ). The $^{143}Nd/^{144}Nd$ using JNDi-1, BCR-1, and W-2 as reference values, JNDi-1 = 0.512115, BCR-1 = 0.512615 ± 121(1σ), W-2 = 0.512519 ± 12(1σ). The analytical results for standard material JNDi-1 = 0.512112, BCR-1 = 0.512629 ± 3(1σ), W-2 = 0.512524 ± 3(1σ), within the allowed deviation range. The results for these standard materials show that the experimental data are reliable (Fig. 3).

4 Analytical results

4.1 Zircon texture, trace element composition, and U–Pb age

In situ zircon U–Pb dating analysis was carried out for the two types of mafic gabbro, and zircon U–Pb geochronology data are presented in Supplementary Table 1. Thirty-six typical zircons were carefully selected from three samples (YM-1, YM-2, YM-3). Discrepant concordant ages of these mafic rocks were obtained and are shown in Fig. 4.

Zircon grains from type 1 mafic gabbro samples display euhedral characteristics, are transparent, colorless, and free of inclusions, and show magmatic oscillatory zoning. In situ zircon U–Pb dating results for type 1 gabbro are shown in Fig. 4a, b and Supplementary Table 1. A total of 18 analyses from sample YM-3 show higher Th and U content ranging from 120.7 to 1774 ppm and 154.3 to 9660 ppm, and Th/U ratios ranging from 0.02 to 1.76, supporting selected zircons originating from plutons (Hoskin and Schaltegger 2003; Wu and Zheng 2004). The dating results for the concordant

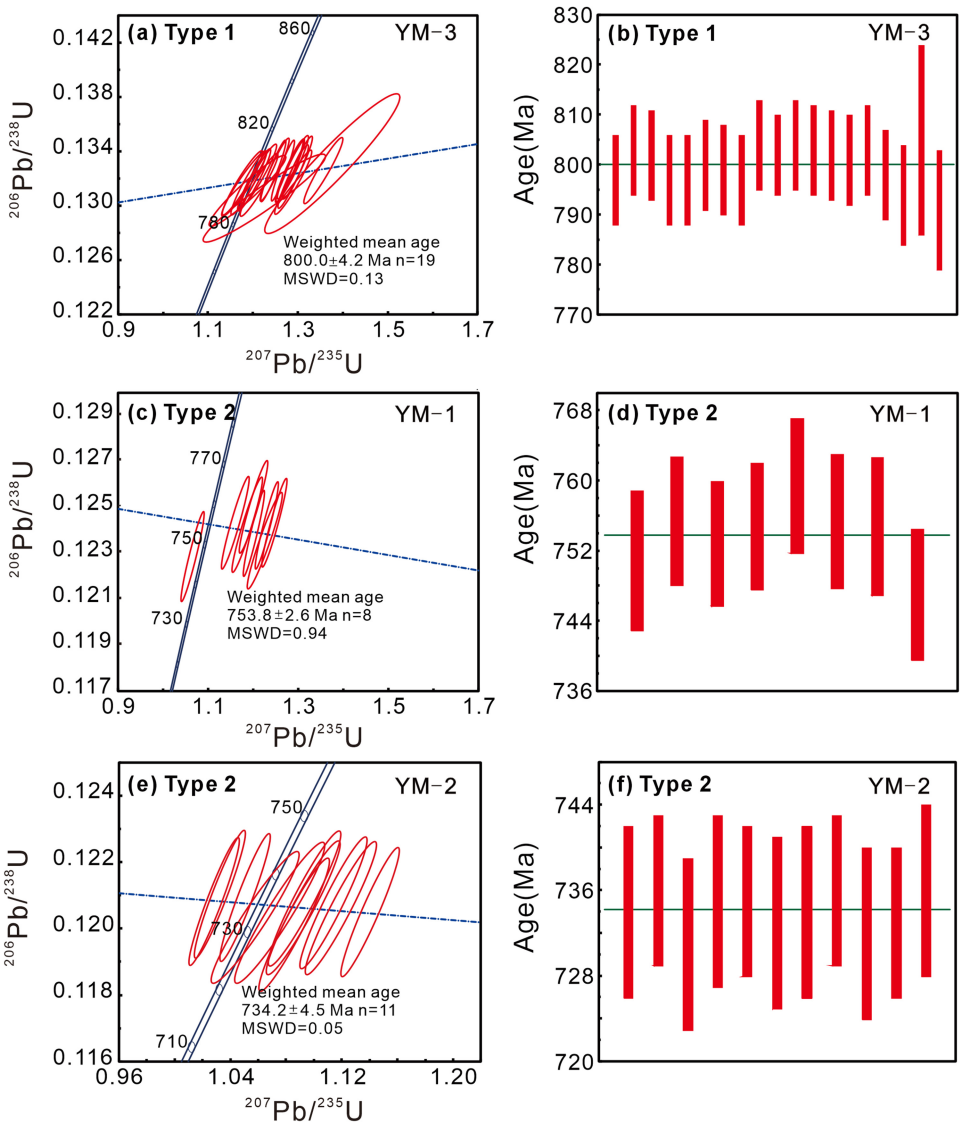

Fig. 3 Laser ablation–inductively coupled plasma mass spectrometry (LA-ICP-MS) U–Pb zircon concordia diagrams for the Early Neoproterozoic mafic gabbros in the western Yangtze Block, South China. **a**, **b** Sample YM-3. **c**, **d** Sample YM-2. **e**, **f** Sample YM-1

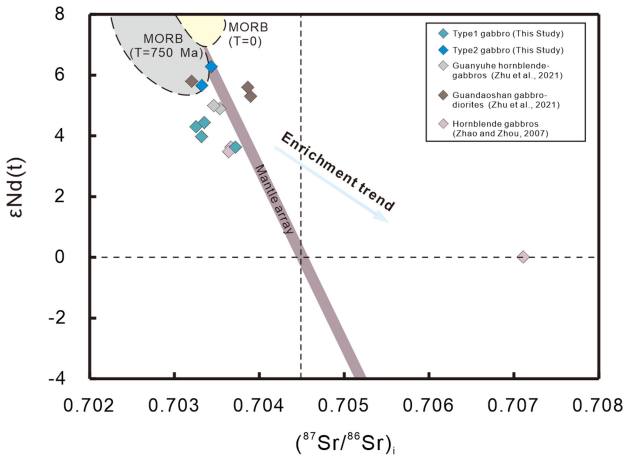

Fig. 4 Classification plots of Zr/TiO2 versus Nb/Y (Winchester and Floyd 1976). The whole-rock data were collected from Zhao and Zhou (2007), Zhu et al. (2021).The mid-ocean ridge basalt (MORB) ($T=0$) and corrected MORB ($T=750$) are from Zimmer et al. (1995)

weighted mean age are 800.0 ± 4.2 Ma (MSWD = 0.13, $n=19$) (Fig. 4a, b).

For type 2 mafic gabbro (YM-1, YM-2), zircon grains show clear, euhedral prismatic characteristics and simple internal growth zoning. Eight analytical spots of YM-1 zircon particles obtained a concordant weighted mean age at 753.8 ± 2.6 Ma (MSWD = 0.94, $n=8$) (Fig. 4c, d). The eight analyzed spots generally display Th (83.5–355 ppm) and U content (167–667 ppm), and Th/U ratios in the range of 0.41–0.81, indicating an igneous origin. Analysis of 10 concordant spots of zircon particles in sample YM-2 shows a concordant weighted mean age of 734.2 ± 4.5 Ma (MSWD = 0.05, $n=11$), younger than type 1 mafic gabbro (Fig. 4e, f). Th/U ratios range from 0.18 to 1.41, consistent with magmatic origin. Magmatic origin is consistent with the confidence Th/U ratio range (0.18–0.41), with measured Th and U content varying from 147 to 6180 ppm and 672 to

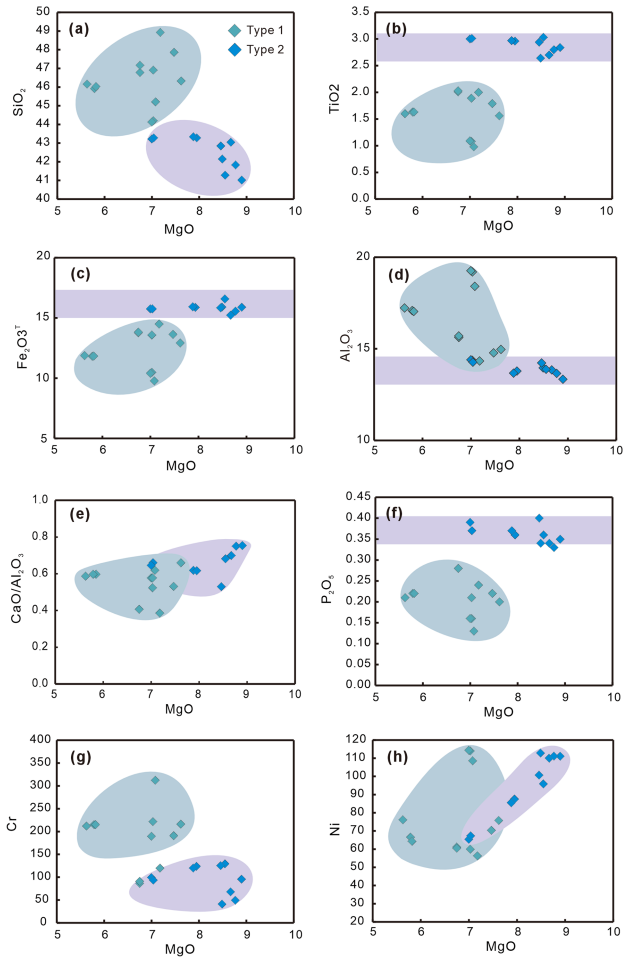

Fig. 5 Harker diagrams of mafic gabbro formed during the Early Neoproterozoic in the western Yangtze Block, South China

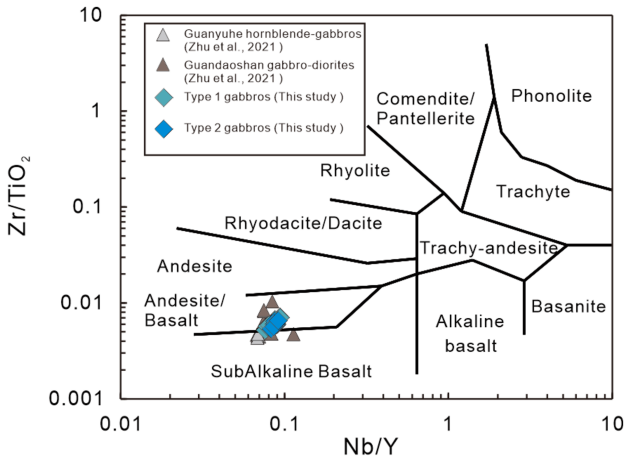

Fig. 7 Plots of La/Sm and Dy/Yb ratios versus SiO_2 (%) for the mafic gabbro in the western Yangtze Block, South China

4380 ppm, respectively (Hoskin and Schaltegger 2003; Wu and Zheng 2004).

4.2 Whole-rock major and trace element geochemistry

The whole-rock major and trace element data for the 22 samples of type 1 gabbro and type 2 gabbro are presented in Supplementary Table 2 and Figs. 4, 5, and 10.

4.2.1 The major and trace element characteristics of type 1 mafic gabbro

A classification diagram of the type 1 mafic gabbro in the andesite/basalt region of the Zr/TiO_2 versus Nd/Y is plotted in Fig. 4 (Winchester and Floyd 1976). Plots of major oxide and trace elements Ni and Cr versus MgO are shown in Fig. 5. Type 1 gabbro contains relatively higher SiO_2 and Al_2O_3 content, lower FeO, MgO, and TiO_2 content, and similar CaO, Ni, and Cr content relative to type 2 gabbro, with SiO_2 = 44.13–47.17 wt%, TiO_2 = 0.98–2.03 wt%, Al_2O_3 = 14.37–19.26 wt%, MgO = 5.63–7.62 wt%, CaO = 5.52–11.39 wt%, $Mg^{\#}$ = 52.5–62.8, Ni = 60.0–114.0 ppm, and Cr = 86.2–312.0 ppm (Supplementary Table 2 and Fig. 5). The SiO_2, Al_2O_3, CaO, and Cr content decreases with increasing MgO content, while $TiO_2$and $Fe_2O_3{}^T$ content shows an increasing trend with increased MgO content (Fig. 6).

In the primitive mantle-normalized trace element diagram, type 1 gabbro exhibits different degrees of positive Ba, U, Sr, and Nd anomalies and negative Nb, Ta, Zr, Hf, and Ti anomalies. Type 1 gabbro has lower total rare earth element content (ΣREE ranges from 139.5 to 289.3 ppm)

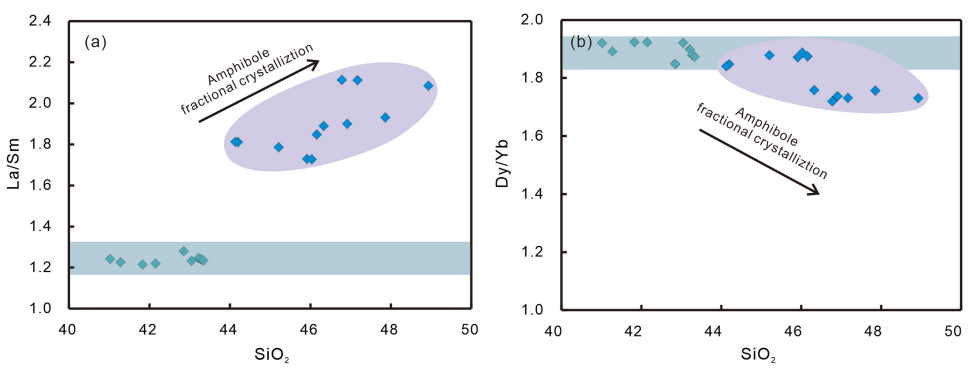

Fig. 6 Plots of $^{87}Sr/^{86}Sr$ versus $\varepsilon Nd(t)$ for the mafic gabbro in the western Yangtze Block, South China. MORB and corrected MORB (T = 750 Ma) data are from Zimmer et al. (1995). The Sr–Nd isotope data for the Early Neoproterozoic mafic magmatism are from Zhao and Zhou (2007) and Zhu et al. (2019)

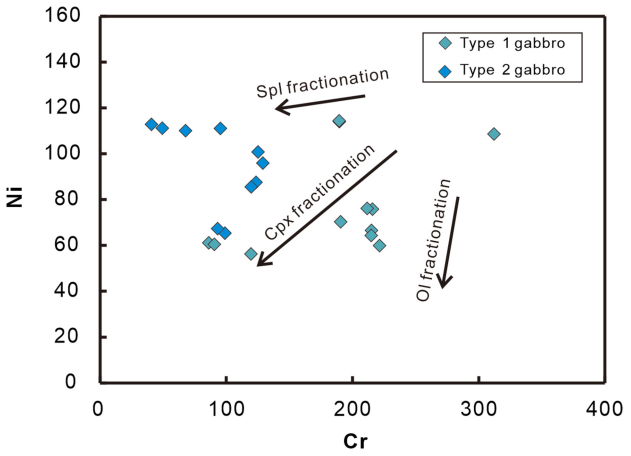

Fig. 8 Plots of Ni versus Cr (ppm) for the mafic gabbro in the western Yangtze Block, South China

than type 2 gabbro (Fig. 10 and Supplementary Table 2). However, rare earth element (REE) chondrite-normalized patterns imply an enriched light rare earth element (LREE) signature, including $(La/Sm)_N$ and $(La/Yb)_N$ ranging from 1.12 to 1.37 and 1.77 to 2.03, respectively (Figs. 7, 8).

4.2.2 The major and trace element characteristics of type 2 mafic gabbro

Type 2 mafic gabbro is all plotted in the region of andesite/basalt in the Zr/TiO_2 versus the Nd/Y classification diagram, indicating the basaltic affinities. (Winchester and Floyd 1976). In contrast to type 1 mafic gabbro, type 2 mafic gabbro has lower SiO_2 = 41.02–43.34 wt% and $Al_2O_{3=}$13.34–14.40 wt%, Cr = 40.8–129 ppm, higher FeO = 15.22–16.57 wt%, and slightly higher TiO_2 = 2.64–3.03 wt.% and $MgO_=$7.00–8.90 wt%, Ni = 67.3–111 ppm (Supplementary Table 2 and Fig. 5). Despite the nearly constant variation in Fe_2O_3, TiO_2, and P_2O_5, the major oxide shows a similar trend versus MgO to that of type 1 gabbro.

Type 2 gabbro exhibits distinct Ba and Pb positive anomalies, slight positive U anomaly, prominent negative Th and Nb anomalies, and different degrees of positive or negative anomalies of REE chondrite-normalized patterns. The diagram shows type 2 gabbro with higher REE (ΣREE range from 266 to 299.7 ppm) and normal mid-ocean ridge basalt (N-MORB)-like REE chondrite-normalized patterns, with $(La/Sm)_N$ and $(La/Yb)_N$ ratios of 0.79–0.83 and 1.34–1.42.

4.3 Whole-rock Sr–Nd isotope geochemistry

The whole-rock Sr–Nd isotopic data for the Yumen mafic–ultramafic rocks in the Yanbian and Xiaoping areas are given in Supplementary Table 3 and Fig. 4. Type 1 and type 2 mafic gabbro both show relatively higher positive εNd(*t*) ranging from 3.3 to 4.4 and 5.6 to 6.3, respectively. The $(^{87}Sr/^{86}Sr)_i$ of type 1 gabbro range from 0.7035–0.7043, which is variable and slightly higher than the initial Sr isotopic ratios of type 2 gabbro (initial $^{87}Sr/^{86}Sr$ = 0.7035–0.7043). Overall, the type 1 mafic gabbro has lower εNd(*t*) than type 2 mafic gabbro but similar initial $^{87}Sr/^{86}Sr$ ratios.

5 Discussion

5.1 Effects of alteration, crustal assimilation, and fractional crystallization

The mafic magma that erupted to the surface will likely have undergone crustal contamination and fractional crystallization. Reevaluating the effect of these magmatic and post-magmatic processes is necessary.

5.1.1 Alteration and crustal assimilation

After emplacement to the surface, mafic rocks are more likely to undergo weathering than acid intrusions; the effect of an alteration should be considered before constraining the potential mantle source of mafic magma. In ultramafic–mafic rocks, loss on ignition (LOI) values (3.25%–5.78%) of mafic rock samples in this study are relatively low. However, assessing the extent of alteration via major and trace element indicators is necessary to guarantee the rationality and validity of the discussion for further identification. The multiple-trace-element diagram of mafic gabbro in this study exhibits near parallel curves, which argues against the variation in elements due to alteration (Fig. 9). In addition, the limited variation in Eu/Eu* (0.88–1.16) and Ce/Ce* (0.90–1.09) suggests insignificant Eu and Ce anomalies, which argue against the mobility of HFSEs and REEs (Polat and Hofmann 2003). Thus, this study's post-magmatic alteration effect of mafic rocks is insignificant, and the geochemical composition may be inherited from the mantle source of mafic gabbro beneath the Western Yangtze Blocks (Fig. 10).

Mantle-derived mafic magmas have potentially undergone crustal contamination during ascent through the continental crust. Continental crust shows higher Rb, Th, and U concentrations (Rb = 84 ppm, Th = 10.5 ppm, and U = 2.7 ppm) relative to primary mantle melts. The lower Rb (average Rb = 2.3 ppm), Th (average Th = 0.36 ppm), and U (U = 0.12 ppm) content present in the newly identified mafic gabbro in this paper argue against extensive

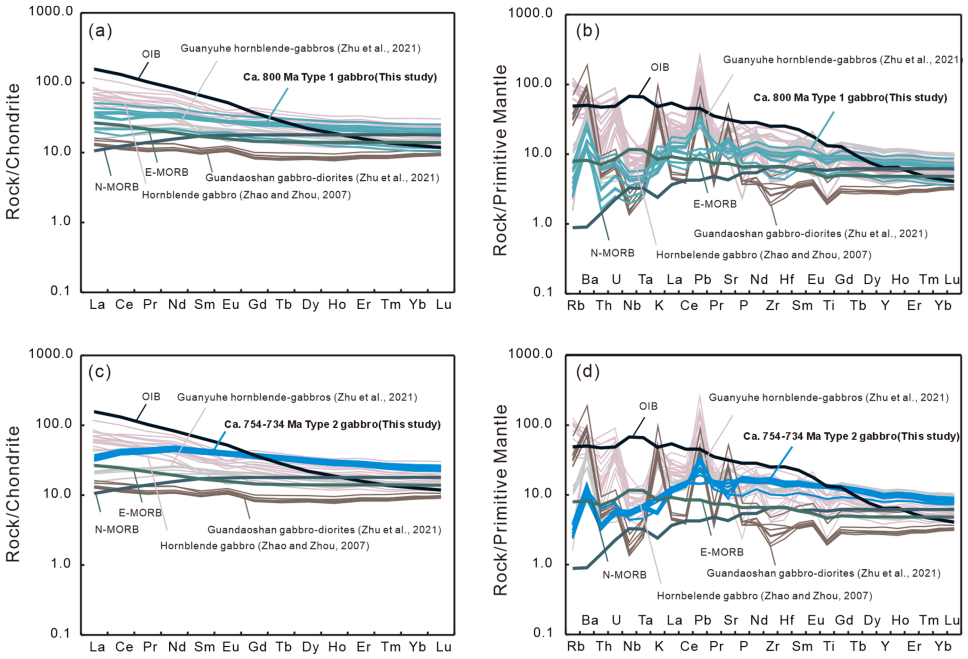

Fig. 9 Chondrite-normalized REE patterns and primitive mantle-normalized incompatible element spidergrams for the Early Neoproterozoic mafic gabbro in the western Yangtze Block, South China. The normalized values for the ocean island basalt (OIB), chondrite, and primitive mantle are from Sun and McDonough (1989). Trace element data for the hornblende gabbro is from Zhao and Zhou (2007). Trace element data for the hornblende Guanyuhe gabbros and Guandaoshan gabbro-diorites are from Zhu et al. (2021)

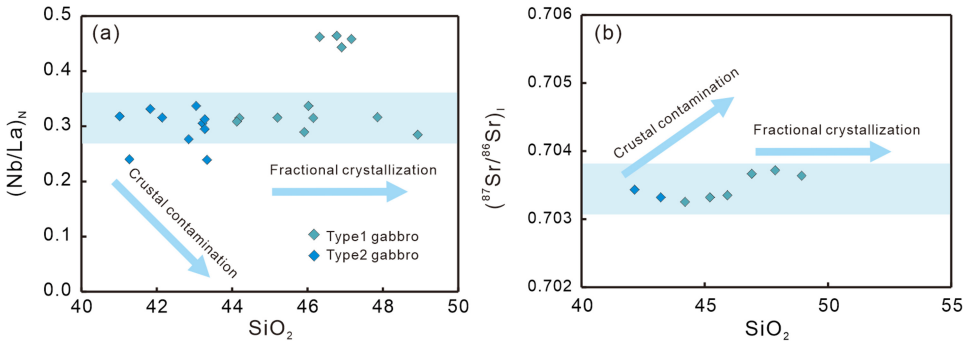

Fig. 10 Plots of $(Nb/La)_N$ versus SiO_2 (**a**) and initial $^{87}Sr/^{86}Sr$ values versus SiO_2 (**b**) for the mafic gabbro in the western Yangtze Block

crustal contamination (Rudnick and Gao 2003) (Supplementary Table 2). Crustal materials are usually enriched in K_2O, Na_2O, and large-ion lithophile element (LILE). Low concentrations of Na_2O and K_2O in type 1 mafic gabbro (2.29–3.64% for Na_2O, 0.16–0.39 for K_2O) and type 2 mafic gabbro (1.90–2.86% for Na_2O, 0.13–0.28% for K_2O) suggest minor crustal contamination for these mafic rocks. The negative Zr-Hf anomalies in type 1 mafic gabbro compared with the slightly positive Zr anomaly and negative Hf anomaly indicate minor crustal contamination (Fig. 9). Furthermore, crustal contamination introduced to magma generally causes La/Sm ratios to decrease and leads to a negative correlation between SiO_2 content and Nb/La ratios (Kou et al. 2018; Zhu et al.2021). The relatively constant Nb/La ratios and narrow $(^{87}Sr/^{86}Sr)_i$ ratios of type 1 gabbro and type 2 gabbro show no correlation with SiO_2, which indicates insignificant crustal assimilation.

The narrow range of $\varepsilon Nd(t)$ values (+3.5–4.4) and $(^{87}Sr/^{86}Sr)_i$ (0.7035–0.7043) ratios for type 1 mafic gabbro, and $\varepsilon Nd(t)$ values (+5.6–6.3) and $(^{87}Sr/^{86}Sr)_i$ (0.7035–0.70436) for type 2 mafic gabbro also supports the minor involvement of crustal materials (Fig. 4 and Supplementary Table 3). Based on the evidence above, minor crustal assimilation was involved in mafic magma during ascent.

5.1.2 *Fractional crystallization*

The fractional crystallization effect during magmatic processes plays an essential role in the evolution of magma. Thus, it may change the abundance of whole-rock major and trace elements during magma evolution. The variable $Mg^{\#}$ (50.89–62.81) and lower Cr and Ni content (67.7–221 ppm and 60.0–111 ppm) relative to the primitive mantle (Fig. 5 and Supplementary Table 2) indicate that both types of mafic gabbro probably experienced fractional crystallization (Sun and McDonough 1989). Primary melts directly derived from mantle generally have Cr > 1000 ppm and

Ni > 400 ppm. The Neoproterozoic mafic rocks in this study with Cr = 40.8–312 ppm and Ni = 56.3–114 ppm indicate the fractional crystallization of olivine and/or clinopyroxene during magma chamber processes or magma ascent (Wilson 1989; Zhao and Zhou 2007; Zhao et al. 2009). Type 1 and type 2 mafic gabbro, as shown in Fig. 5, show a near positive correlation between Ni, Cr, and MgO content, and a slight positive correlation for CaO/Al_2O_3 ratios and MgO content, indicating olivine and/or clinopyroxene fractional crystallization. In the diagrams of Cr versus Ni (Fig. 5g–h), type 1 gabbro shows a tendency for olivine/clinopyroxene fractionation. In contrast, type 2 gabbro exhibits spinel and clinopyroxene fractionation trends (Fig. 8). The positive correlation shown with La/Sm and SiO_2 and the decreasing Dy/Yb ratios varying with increasing SiO_2 content for the type 2 gabbro support the fractionation of amphibole in their magma source (Fig. 7). The prominent negative correlation between Al_2O_3 and MgO content (Fig. 5d) and the slight negative Eu anomalies (Fig. 10) may support the minor accumulation of plagioclase. Figure 5b and c illustrate the differences between type 1 and type 2 mafic gabbro. Type 1 mafic gabbro demonstrates a slight crystallization of Fe oxides and Ti oxides, which is reflected in a positive correlation among $Fe_2O_3^T$, MgO, and TiO_2 content. In contrast, type 2 mafic gabbro exhibits relatively constant levels of $Fe_2O_3^T$ and TiO_2 in relation to MgO content, indicating that the fractional crystallization of Fe and Ti oxides is negligible. The relatively low Na_2O and K_2O concentrations in both types of mafic gabbro suggest an absence of hornblende fractionation, which is also supported by the petrology under microscopic observation (Fig. 2 and Supplementary Table 1). Thus, fractional crystallization plays an essential role in magma evolution.

5.2 Nature of the mantle source: the long-term metasomatism revealed by 800–730 Ma mafic dykes in the western Yangtze Block

5.2.1 The long-term subduction-related metasomatism

Both types of mafic gabbro (800 Ma for type 1 mafic gabbro and 753–734 Ma for type 2 mafic gabbro) in this study show lower SiO_2 (41.02–48.93%) and relatively high MgO (5.63–8.90 wt%) and $Mg^{\#}$ values (50.89–62.81) (Supplementary Table 2), which suggests they may originate from a depleted mantle source (Wilson 1989). The type 1 mafic gabbro shows higher SiO_2, Al_2O_3, and CaO content but lower MgO, Cr, and Ni content than the type 2 mafic gabbro. Considering their notably depleted εNd(t) (3.5–4.4 for type 1, and 5.6–6.3 for type 2) and limited range of $(^{87}Sr/^{86}Sr)_i$ values (0.7035–0.7040 for type 1, and 0.7035–0.7036 for type 2) (Supplementary Table 3 and Fig. 4), the similarity between our mafic gabbro samples and Neoproterozoic mafic plutons (e.g., Gundaoshan pluton, Baoxing pluton) suggests a depleted lithospheric mantle source signature (Sun and Zhou 2008; Yang et al. 2017; Zhao and Zhou 2009; Zhu et al. 2008; Zhao et al. 2019). Incompatible elements tend to enrich in melt during partial melting processes, and mantle-derived melts (e.g., MORB) usually have lower concentrations of incompatible elements (Fig. 9; Sun and McDonough 1989). Moreover, mafic gabbro exhibits enriched trace elements, including Rb, Ba, Sr, U, K, La, and Pb (LILE and LREE), and depletion in Nd, Ta, Zr, Hf, and Ti (HFSEs), which demonstrates arc-like trace element features associated with magmas derived from metasomatized mantle (Fig. 9; Sun and McDonough 1989; Cervantes and Wallace 2003; Zhao and Zhou 2007, 2009). Trace element and Sr–Nd isotope features combined with alteration and crustal assimilation discussed above suggest that the enriched signature probably inherited from the mantle source experienced metasomatism correlated with the penetration of subduction material before its partial melting.

Sediment melts, slab melts, and fluids derived from subduction processes are introduced into the mafic source, contributing to the generation of arc-like ultramafic–mafic rocks (Hanyu et al. 2006; Kepezhinskas et al. 1997; Hacker et al. 2003; Zhou et al. 2006). Magmas in the margins of continent and plate boundaries are mostly generated from mantle wedge modified by subduction materials (e.g., subduction-related fluid, subduction-related melt) (Zhao and Zhou 2009). The type 1 gabbro yielded $(Hf/Sm)_N$ versus $(Ta/La)_N$ ratios of 0.73–0.94 and 0.33–0.37, with type 2 gabbro showing comparably higher $(Hf/Sm)_N$ (0.93–1.12) and $(Ta/La)_N$ ratios (0.55–0.58), indicating a slab-derived fluid metasomatism trend in the $(Hf/Sm)_N$ versus $(Ta/La)_N$ diagram (Fig. 11a). Previous research on mafic subduction-derived metasomatism agents demonstrated that slab melts generally exhibit high Th and LREE content; the low Th content (0.14–0.73 ppm) and low Th/La ratios (0.029–0.061) found in mafic gabbro in this study suggest an insignificant role of subduction-related melt involved in both types of mafic gabbro (Supplementary Table 2, Figs. 9 and 11b). They yield high Ba/La (7.8–23.4) and notably high Ba/Th (143.7–444.7) ratios, implying prominent introduced components of subduction-related fluid rather than subduction-related melt. The type 1 gabbro in this study displayed variations in Th/Zr values (0.003–0.005) and Nb/Zr values (0.026–0.028), whereas type 2 gabbro exhibited constant Th/Zr ratios (~0.002) and variable Nb/Zr ratios (0.021–0.022), which combined with negative anomalies of Nb in Fig. 9 and the increasing trend of Th/Zr ratios indicate the slab-derived fluid trend of type 1 and type 2 mafic gabbro (Fig. 11b). In addition, the high Ba/Nb ratios (16.31–71.86) of both types of gabbro relative to N-MORB (Ba/Nb = 0.28) and E-MORB (Ba/Nb = 0.71), which is correspondingly approximate to the continental crust (Ba/Nb = 51.8–52.3), also suggest a certain extent of slab-derived fluid metasomatism (Rudnick and Gao 2003; Sun and McDonough 1989; Zhao and Zhou 2009; Zhao

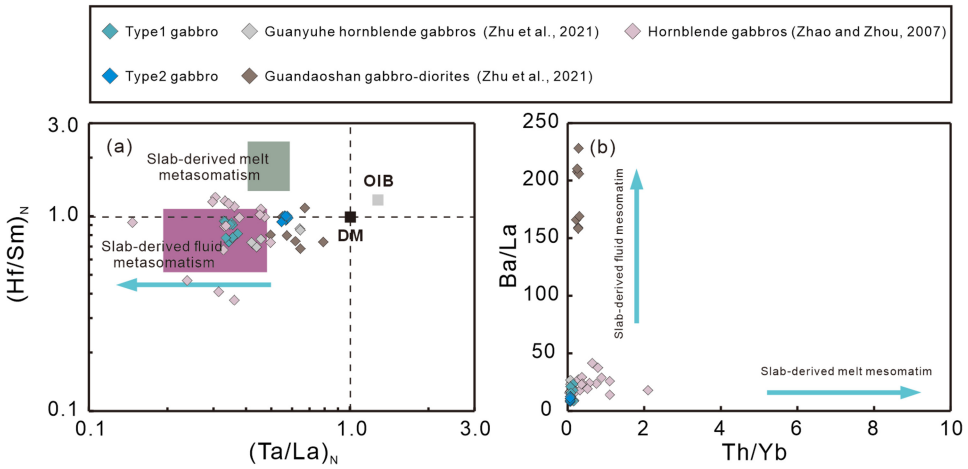

Fig. 11 Plots of $(Hf/Sm)_N$ versus $(Ta/La)_N$ (La Flèche et al. 1998) (**a**), Nb/Zr versus Th/Zr (Kepezhinskas et al. 1997) (**b**), Rb/Y versus Nb/Y (Kepezhinskas et al. 1997) (**c**), and Ba/La versus Th/Yb (Hanyu et al. 2006) (**d**) for the Neoproterozoic mafic rocks in the western Yangtze Block, South China

et al. 2019). In the Rb/Y versus Nb/Y diagrams, variable Rb/Y ratios with a narrow range of Nb/Y ratios suggest a metasomatic trend along with subduction-related fluid enrichment (Fig. 11c). The variability in Ba/La ratios (7.80–23.36) compared with low and nearly constant Th/Yb (0.07–0.17) and Th/Nb (0.01–0.04) ratios further supports a more significant input of subduction-related fluids than subduction-related melt for the modified origin (Hanyu et al. 2006; Xu et al. 2019) (Fig. 11d). Therefore, the above geochemical features of mafic gabbro suggest that type 1 and type 2 mafic gabbro with inherited depleted chemistry both originate from a metasomatized source, and underwent variable degrees of slab-derived fluid metasomatism; the type 1 mafic gabbro combined with indicators above may have undergone stronger subduction-related fluid metasomatism than type 2 mafic gabbro.

5.2.2 *Petrology and nature of the mantle: implications from subduction-related metasomatism modification*

The long-term magma events in the western Yangtze Block, South China, formed many Neoproterozoic felsic plutonic rocks and minor ultramafic–mafic rocks (Du et al. 2014; Yang et al. 2017; Zhao and Zhou 2007, 2009; Zhao et al. 2019; Zhou et al. 2006; Zhu et al. 2008). Li et al. (2002, 2003, 2006) ascribed the genesis of some mafic rocks in the western margin of the Yangtze Block with OIB features to the effects of mantle plume activity, which is inconsistent with our arc affinity results for mafic gabbro. The typical OIB-derived mafic melts generally have Zr/Nb (Zr/Nb = 5.83), and the possibility of an OIB source can be ruled out with the higher Zr/Nb (35.76–46.91) in our Neoproterozoic mafic gabbro (Sun and McDonough 1989). The 800 Ma type 1 gabbro and 753–743 Ma type 2 gabbro yield approximately constant depleted εNd(t) (3.47–4.43 and 5.65–6.27) and $^{87}Sr/^{86}Sr$ (0.7033–0.7037 and 0.7033–0.7034) along with variable Ba/Nb, $(Hf/Sm)_N$, $(Ta/La)_N$, Nb/Zr, Th/Zr, Rb/Y, Ba/La, and Th/Y ratios, and trace element characteristics suggest the same depleted source which was metasomatized by subduction-related fluids (Kepezhinskas et al. 1997; Zhao and Zhou 2007; Zhu et al. 2021)(Figs. 6 and 11, 12). The potential magma origin of mafic rocks in the western margin of the Yangtze Block, South China, was ascribed as follows: The arc-like and N-MORB-like trace element signature mafic rocks were spatially distributed in the western margin of the Yangtze Block from 870 to 740 Ma; those magma events suggest the recycling of crustal materials by subduction into the mantle source beneath the western Yangtze Block (Yang et al. 2017; Zhao and Zhou 2007, 2009;

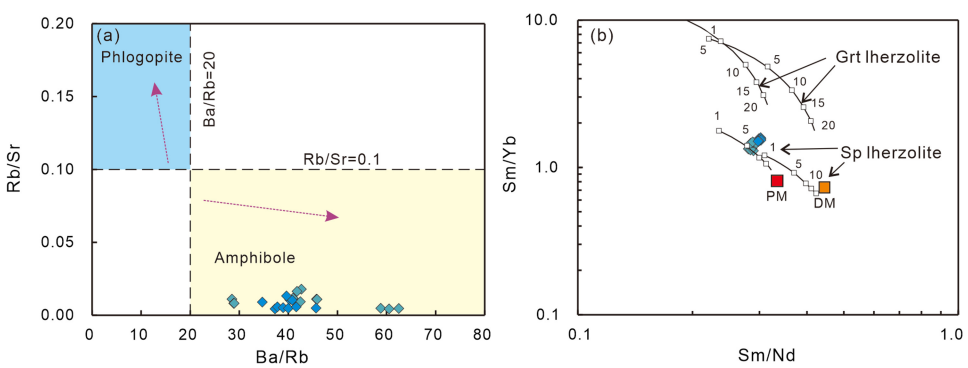

Fig. 12 Plots of Rb/Sr versus Ba/Rb (**a**) and Sm/Yb versus Sm/Nd (**b**) for both types of mafic gabbro in the western margin of the Yangtze Block, South China

Zhao et al. 2019; Zhou et al. 2006; Zhu et al. 2008, 2021). The prolonged mantle metasomatism in the source of mafic gabbro in this study mainly consists of subduction-related fluid metasomatism, which suggests the existence of hydro-minerals (e.g., amphiboles) in the metasomatized source (Xu et al. 2019). In contrast to phlogopite-bearing sources, mantle sources with amphibole usually display higher Ba/Rb and lower Rb/Sr ratios. The trend of decreasing Rb/Sr with increasing Ba/Rb ratios indicates hydro-minerals mainly consisting of amphibole (Fig. 12a). The potential magma source for both type 1 and type 2 mafic gabbro is common spinel-lherzolite, in contrast to garnet lherzolite, due to the flat heavy rare earth element (HREE) curve in the chondrite-normalized diagram of REEs. These mafic gabbro are probably sourced from proximately 5%–10% partial melting of metasomatized spinel lherzolite, but type 2 mafic gabbro may originate from deeper depths with higher Sm/Yb and Sm/Nd ratios (Figs. 9 and 12b). Although the different partial melting can produce different types of magma, the trace elements and Sr–Nd isotopes remain original; thus, the type 1 and type 2 mafic gabbro derived from different magma sources [variable $\varepsilon Nd(t)$ and initial $^{87}Sr/^{86}Sr$] demonstrate similar petrology of source and metasomatized geochemical features (enriched LILE, depleted HFSE). Subduction-related metasomatism is likely to play a significant role in the mantle source. This influence stems from two main factors: the comparable degree of partial melting observed in the source's mafic gabbro and the wide range of La/Sm ratios identified in both types of mafic gabbro. Integrating the evidence presented above, it can be concluded that slab-derived fluid metasomatism significantly impacts the petrology of the mantle source located beneath the western margin of the Yangtze Block. Additionally, the formation of the mafic gabbro investigated in this study is closely linked to the partial melting of metasomatized spinel lherzolite by subduction-related fluid.

5.3 Implications for the tectonic settings during 800–730 Ma via long-term mafic magma events

Previous research holds that plume setting and mantle plume model are responsible for the genesis of diverse igneous rocks in the west margin of the Yangtze Block (Li et al. 2002, 2003, 2006; Wu et al. 2019). The long-term magmatic events (860–740 Ma) in the western Yangtze Block are distinct from the mantle plume magmatic events (1–5 Ma) in time scale (Campbell 2007; Shellnutt 2014; Xu et al. 2014). In addition, mantle plume-induced magmatic events are identified with a large-scale distribution of ultramafic–mafic rocks in short intervals (Shellnutt 2014; Xu et al. 2014). These mafic rocks exhibit a typical OIB-like geochemical composition (Shellnutt 2014; Xu et al. 2014). The above features of large igneous provinces (LIPs) lack long-term magmatic events and demonstrate limited ultramafic–mafic rock distributions in the western Yangtze Block. Zhou et al. (2006) proposed the Panxi-Hannan arc across the Yanbian terrane to the Hannan region of about 1000 km, and this arc system existed for about 100 Ma (from 840 to 750 Ma), which was further proved by Zhao et al. (2019). Thus, this study's tectonic background of mafic gabbro is related to arc settings (Zhao and Zhou 2007; Zhao et al. 2019; Zhou et al. 2006).

The 800 and 750 Ma adakitic-affinity granitic plutons and widespread mafic plutons with arc-like geochemical signatures during 860–740 Ma also support the active subduction process that occurred in the west margin of the Yangtze Block during the Neoproterozoic time (Zhao and Zhou 2007, 2009; Zhao et al. 2019; Zhou et al. 2006; Zhu et al. 2008, 2019, 2021) (Fig. 1b). Subduction-related rock sequences are consistent in the Yanbian terrane, which consists of a back-arc volcanic sedimentary sequence in the north part of the Panxi region (Zhou et al. 2006; Zhu et al. 2019). Thus, we believe the arc setting to be more reasonable than the mantle plume setting; this arc system that existed during 840–750 Ma may be responsible for the mafic magmatism and adakite that emerged in the western margin of the Yangtze Block.

The arc-related signatures (e.g., enriched LILE, e.g., Ba, Rb, K, Pb, depleted HFSE, e.g., Nb, Ta, Zr, Hf, Ti) of type 1 and type 2 mafic gabbro in the western Yangtze Block during the Early Neoproterozoic are observed in this study. In the subduction-related setting, interactions between the slab-derived fluid and overlying mantle wedge lead to the enriched mantle origin at sub-arc depths, generating mafic rocks with depleted isotopic geochemical features and enriched trace element characteristics (Kelemen et al. 2014; Zheng et al. 2020). This is consistent with the Neoproterozoic mafic gabbro in this study in the western Yangtze Block, with LILE enrichment and depleted HFSEs (Fig. 9). The magma source and mantle metasomatic processes associated with type 1 and type 2 mafic gabbro are evidenced by close

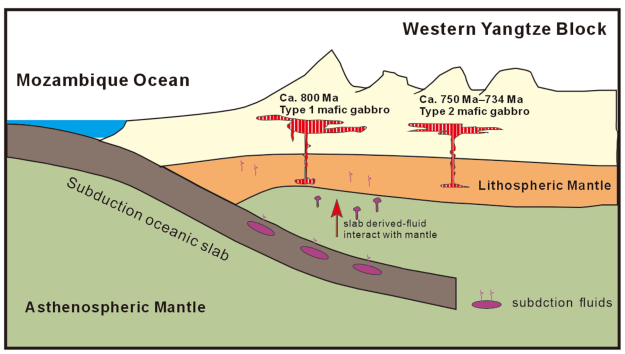

Fig. 13 Tectonic model for the subduction beneath the western margin of the Yangtze Block during the Neoproterozoic

εNd(t) values and approximate geochemical trace element features of subduction fluid metasomatism. We suggest that these mafic gabbro are formed in the back-arc rift setting; the subduction slab subducted into the mantle wedge at about 870 Ma, then slab tearing occurred at about 820 Ma, the slab released subduction-related fluids which strongly metasomatized the surrounding mantle, finally generating the mafic plutons in the western margin of the Yangtze Block (Cawood et al. 2016; Zhao et al. 2019). The identification of 800 and 734 Ma Yumen mafic gabbro in this study strongly supports the long-term subduction-related fluid metasomatism that existed beneath the western margin of the Yangtze Block, South China. Previous studies of ultramafic–mafic rocks in this region also support the important role of subduction melt, sediments, and fluid in the formation and generation of these subduction-related mafic rocks during the Early Neoproterozoic (~ 860–730 Ma) (Yang et al. 2017; Zhao and Zhou 2007, 2009; Zhao et al. 2019; Zhou et al. 2006; Zhu et al. 2008, 2021) (Fig. 13).

6 Concluding remarks

The zircon U–Pb geochronological results show that the newly identified Neoproterozoic Yumen mafic gabbro in the western Yangtze Block formed at ca. 800 Ma and 750–734 Ma. Combined with the whole-rock major–trace element results and Sr–Nd isotopic data, this indicates a prolonged subduction-related fluid metasomatism of magma source beneath the western margin of the Yangtze Block, South China. This study with new data of newly identified mafic gabbro (ca. 800–734 Ma) in the western margin of the Yangtze Block further supports the important role of subduction components in the generation of diverse ultramafic–mafic magma during the Early Neoproterozoic, which enhances our understanding of subduction-related metasomatic processes in arc-related settings during the Neoproterozoic.

Acknowledgements The National Natural Science Foundation of China [Grant Nos. 42172056, 42202048] co-supported this work.

Author contributions ZZ: field investigation, data analyses and the manuscript writing; SL: supervising and funding; YZ: study design and manuscript revising; JQ: supervising; RZ: supervising; ML: supervising; YX: field investigation.

Declarations

Conflict of interest The authors declare that they have no conflict of interest.

References

Andersen T (2002) Correction of common lead in U-Pb analyses that do not report 204Pb. Chem Geol 192(1–2):59–79. https://doi.org/10.1016/S0009-2541(02)00195-X

Barry TL, Pearce JA, Leat PT, Millar IL, le Roex AP (2006) Hf isotope evidence for selective mobility of high-field-strength elements in a subduction setting: South Sandwich Islands. Earth Planet Sci Lett 252(3–4):223–244. https://doi.org/10.1016/j.epsl.2006.09.034

Campbell IH (2007) Testing the plume theory. Chem Geol 241(3–4):153–176. https://doi.org/10.1016/j.chemgeo.2007.01.024

Cawood PA, Strachan RA, Pisarevsky SA, Gladkochub DP, Murphy JB (2016) Linking collisional and accretionary orogens during Rodinia assembly and breakup: Implications for models of supercontinent cycles. Earth Planet Sci Lett 449:118–126. https://doi.org/10.1016/j.epsl.2016.05.049

Cervantes P, Wallace PJ (2003) Role of H_2O in subduction-zone magmatism: new insights from melt inclusions in high-Mg basalts from central Mexico. Geology 31(3):235. https://doi.org/10.1130/0091-7613(2003)0310235:rohois%3e2.0.co;2

Davidson JP (1987) Crustal contamination versus subduction zone enrichment: examples from the Lesser Antilles and implications for mantle source compositions of island arc volcanic rocks. Geochim Cosmochim Acta 51(8):2185–2198. https://doi.org/10.1016/0016-7037(87)90268-7

Du LL, Guo JH, Nutman AP, Wyman D, Geng YS, Yang CH, Liu FL, Ren LD, Zhou XW (2014) Implications for Rodinia reconstructions for the initiation of neoproterozoic subduction at ~860Ma on the western margin of the Yangtze block: evidence from the guandaoshan pluton. Lithos 196:67–82. https://doi.org/10.1016/j.lithos.2014.03.002

Greentree MR, Li ZX, Li XH, Wu HC (2006) Late Mesoproterozoic to earliest Neoproterozoic basin record of the Sibao orogenesis in western South China and relationship to the assembly of Rodinia. Precambrian Res 151(1–2):79–100. https://doi.org/10.1016/j.precamres.2006.08.002

Grove T, Parman S, Bowring S, Price R, Baker M (2002) The role of an H_2O-rich fluid component in the generation of primitive basaltic andesites and andesites from the Mt. Shasta region, N California. Contrib Mineral Petrol 142(4):375–396. https://doi.org/10.1007/s004100100299

Hacker BR, Abers GA, Peacock SM (2003) Subduction factory 1. Theoretical mineralogy, densities, seismic wave speeds, and H_2O contents. J Geophys Res 108(B1):2001JB001127. https://doi.org/10.1029/2001jb001127

Hanyu T, Tatsumi Y, Nakai S, Chang Q, Miyazaki T, Sato K, Tani K, Shibata T, Yoshida T (2006) Contribution of slab melting and slab dehydration to magmatism in the NE Japan arc for the last 25 Myr: constraints from geochemistry. Geochem Geophys Geosyst 7(8):Q08002. https://doi.org/10.1029/2005GC001220

Hoskin PWO, Schalategger U (2003) The composition of zircon and igneous and metamorphic petrogenesis. Rev Mineral Geochem 53(1):27–62. https://doi.org/10.2113/0530027

Kepezhinskas P, McDermott F, Defant MJ, Hochstaedter A, Drummond MS, Hawkesworth CJ, Koloskov A, Maury RC, Bellon H (1997) Trace element and Sr–Nd–Pb isotopic constraints on a three-component model of Kamchatka Arc petrogenesis. Geochim Cosmochim Acta 61(3):577–600. https://doi.org/10.1016/S0016-7037(96)00349-3

Kelemen PB, Hanghøj K, Greene AR (2014) One view of the geochemistry of subduction-related magmatic arcs, with an emphasis on primitive andesite and lower crust. In: Treatise on geochemistry. Elsevier, pp 749–806. https://doi.org/10.1016/b978-0-08-095975-7.00323-5

Kou CH, Liu YX, Huang H, Li TD, Ding XZ, Zhang H (2018) The Neoproterozoic arc-type and OIB-type mafic-ultramafic rocks in the western Jiangnan Orogen: implications for tectonic settings. Lithos 312–313:38–56. https://doi.org/10.1016/j.lithos.2018.05.004

Munteanu M, Wilson A, Yao Y, Harris C, Chunnett G, Luo Y, (2010) The Tongde dioritic pluton (Sichuan, SW China) and its geotectonic setting: Regional implications of a local-scale study. Gond Res 18(2):455–465. http://doi.org.10.1016/j.gr.2010.01.005

La Flèche MR, Camiré G, Jenner GA (1998) Geochemistry of post-Acadian, Carboniferous continental intraplate basalts from the Maritimes Basin, Magdalen Islands, Québec, Canada. Chem Geol 148(3–4):115–136. https://doi.org/10.1016/S0009-2541(98)00002-3

Liu Y, Liu XM, Hu ZC, Diwu CR, Yuan HL, Gao S (2007) Evaluation of accuracy and long-term stability of determination of 37 trace elements in geological samples by ICP-MS. Acta Petrol Sin 23(5):1203–1210 (**in Chinese with English abstract**)

Li XH, Li ZX, Zhou HW, Liu Y, Kinny PD (2002) U-Pb zircon geochronology, geochemistry and Nd isotopic study of Neoproterozoic bimodal volcanic rocks in the Kangdian Rift of South China: implications for the initial rifting of Rodinia. Precambrian Res 113(1–2):135–154. https://doi.org/10.1016/S0301-9268(01)00207-8

Li XH, Li ZX, Zhou HW, Liu Y, Liang XR, Li WX (2003) SHRIMP U-Pb zircon age, geochemistry and Nd isotope of the Guandaoshan pluton in SW Sichuan: petrogenesis and tectonic significance. Sci China Ser D Earth Sci 46(1):73–83. https://doi.org/10.1360/03dz9029

Li XH, Li ZX, Sinclair JA, Li WX, Carter G (2006) Revisiting the "Yanbian Terrane": implications for neoproterozoic tectonic evolution of the western Yangtze Block, South China. Precambrian Res 151(1–2):14–30. https://doi.org/10.1016/j.precamres.2006.07.009

Ludwig KR (2003) Isoplot 3.0: a geochronological toolkit for Microsoft Excel. Berkeley Geochronology Center, Special Publication, No. 4

Meng E, Liu FL, Du LL, Liu PH, Liu JH (2015) Petrogenesis and tectonic significance of the Baoxing granitic and mafic intrusions, southwestern China: evidence from zircon U-Pb dating and Lu–Hf isotopes, and whole-rock geochemistry. Gondwana Res 28(2):800–815. https://doi.org/10.1016/j.gr.2014.07.003

Plank T, Langmuir CH (1998) The chemical composition of subducting sediment and its consequences for the crust and mantle. Chem Geol 145(3–4):325–394. https://doi.org/10.1016/S0009-2541(97)00150-2

Peacock SM (1990) Fluid processes in subduction zones. Science 248(4953):329–337. https://doi.org/10.1126/science.248.4953.329

Polat A, Hofmann AW (2003) Alteration and geochemical patterns in the 3.7–3.8 Ga Isua greenstone belt, West Greenland. Precambrian Res 126(3–4):197–218. https://doi.org/10.1016/S0301-9268(03)00095-0

Rudnick RL, Gao S (2003) Composition of the continental crust. In: Rudnick RL (ed) Treatise on geochemistry. Elsevier, New York, pp 1–64. https://doi.org/10.1016/b0-08-043751-6/03016-4

Shellnutt JG (2014) The Emeishan large igneous province: a synthesis. Geosci Front 5(3):369–394. https://doi.org/10.1016/j.gsf.2013.07.003

Sun SS, McDonough WF (1989) Chemical and isotopic systematics of oceanic basalts: Implications for mantle composition and processes. In: Saunders AD, Norry MJ (eds) Magmatism in the Ocean Basins, vol 42, no. 1. Geol Soc Lond Spec Publ, pp 313–345. https://doi.org/10.1144/gsl.sp.1989.042.01.19

Sun WH, Zhou MF (2008) The ~860 Ma, cordilleran-type Guandaoshan dioritic pluton in the Yangtze Block, SW China: Implications for the origin of Neoproterozoic magmatism. J Geol 116(3):238–253. https://doi.org/10.1086/587881

Tatsumi Y (1989) Migration of fluid phases and genesis of basalt magmas in subduction zones. J Geophys Res Solid Earth 94(B4):4697–4707

Wiedenbeck M, Hanchar JM, Peck WH, Sylvester P, Valley J, Whitehouse M, Kronz A, Morishita Y, Nasdala L, Fiebig J, Franchi I, Girard JP, Greenwood RC, Hinton R, Kita N, Mason PRD, Norman M, Ogasawara M, Piccoli PM, Rhede D, Satoh H, Schulz-Dobrick B, Skår O, Spicuzza M, Terada K, Tindle A, Togashi S, Vennemann T, Xie Q, Zheng YF (2004) Further characterisation of the 91500 zircon crystal. Geostand Geoanalyt Res 28(1):9–39. https://doi.org/10.1111/j.1751-908x.2004.tb01041.x

Winchester JA, Floyd PA (1976) Geochemical magma type discrimination: application to altered and metamorphosed basic igneous rocks. Earth Planet Sci Lett 28(3):459–469. https://doi.org/10.1016/0012-821x(76)90207-7

Wilson M (1989) Igneous petrogenesis. Unwin Hyman, London, pp 191–373

Wu YB, Zheng YF (2004) Genesis of zircon and its constraints on interpretation of U-Pb age. Chin Sci Bull 49(15):1554–1569. https://doi.org/10.1007/BF03184122

Wu T, Wang XC, Li WX, Wilde SA, Tian LY (2019) Petrogenesis of the ca. 820–810 Ma felsic volcanic rocks in the Bikou Group: implications for the tectonic setting of the western margin of the Yangtze Block. Precambrian Res 331:105370. https://doi.org/10.1016/j.precamres.2019.105370

Xu YG, Wei X, Luo ZY, Liu HQ, Cao J (2014) The Early Permian Tarim large igneous province: main characteristics and a plume incubation model. Lithos 204(3):20–35. https://doi.org/10.1016/j.lithos.2014.02.015

Xu W, Zhu DC, Wang Q, Weinberg RF, Wang R, Li SM, Zhang LL, Zhao ZD (2019) Constructing the Early Mesozoic Gangdese crust in southern Tibet by hornblende-dominated magmatic differentiation. J Petrol 60(3):515–552. https://doi.org/10.1093/petrology/egz005

Yang YJ, Zhu WG, Bai ZJ, Zhong H, Ye XT, Fan HP (2017) Petrogenesis and tectonic implications of the Neoproterozoic Datian mafic–ultramafic dykes in the Panzhihua area, western Yangtze Block, SW China. Int J Earth Sci 106(1):185–213. https://doi.org/10.1007/s00531-016-1310-7

Yuan HL, Gao S, Liu XM, Li HM, Gunther D, Wu FY (2004) Accurate U-Pb age and trace element determinations of zircon by laser ablation-inductively coupled plasma mass spectrometry. Geostand Geoanal Res 28(3):353–370

Zimmer M, Kroner A, Jochum KP, Reischmann T, Todt W (1995) The Gabal Gerf complex: A precambrian N-MORB ophiolite in the Nubian Shield, NE Africa. Chem Geo 123(1-4):29–51. http://doi.org/10.1016/0009-2541(95)00018-H

Zhao GC, Cawood PA (2012) Precambrian geology of China. Precambrian Res 222:13–54. https://doi.org/10.1016/j.precamres.2012.09.017

Zhao JH, Zhou MF (2007) Geochemistry of Neoproterozoic mafic intrusions in the Panzhihua district (Sichuan Province, SW China): Implications for subduction-related metasomatism in the upper mantle. Precambrian Res 152(1–2):27–47. https://doi.org/10.1016/j.precamres.2006.09.002

Zhao JH, Zhou MF (2009) Secular evolution of the Neoproterozoic lithospheric mantle underneath the northern margin of the Yangtze Block, South China. Lithos 107(3–4):152–168. https://doi.org/10.1016/j.lithos.2008.09.017

Zhao JH, Li QW, Liu H, Wang W (2018) Neoproterozoic magmatism in the western and northern margins of the Yangtze Block (South China) controlled by slab subduction and subduction-transform-edge-propagator. Earth Sci Rev 187:1–18. https://doi.org/10.1016/j.earscirev.2018.10.004

Zhao JH, Zhou MF, Wu YB, Zheng JP, Wang W (2019) Coupled evolution of Neoproterozoic arc mafic magmatism and mantle wedge in

the western margin of the South China Craton. Contrib Mineral Petrol 174(4):36. https://doi.org/10.1007/s00410-019-1573-7

Zheng YF, Xiao WJ, Zhao GC (2013) Introduction to tectonics of China. Gondwana Res 23(4):1189–1206. https://doi.org/10.1016/j.gr.2012.10.001

Zheng YF, Xu Z, Chen L, Dai LQ, Zhao ZF (2020) Chemical geodynamics of mafic magmatism above subduction zones. J Asian Earth Sci 194:104185. https://doi.org/10.1016/j.jseaes.2019.104185

Zhou MF, Ma YX, Yan DP, Xia XP, Zhao JH, Sun M (2006) The Yanbian terrane (southern Sichuan Province, SW China): A Neoproterozoic arc assemblage in the western margin of the Yangtze Block. Precambrian Res 144(1–2):19–38. https://doi.org/10.1016/j.precamres.2005.11.002

Zhu WG, Zhong H, Li XH, Deng HL, He DF, Wu KW, Bai ZJ (2008) SHRIMP zircon U-Pb geochronology, elemental, and Nd isotopic geochemistry of the Neoproterozoic mafic dykes in the Yanbian area, SW China. Precambrian Res 164(1–2):66–85. https://doi.org/10.1016/j.precamres.2008.03.006

Zhu WG, Zhong H, Li ZX, Bai ZJ, Yang YJ (2016) SIMS zircon U-Pb ages, geochemistry and Nd–Hf isotopes of ca. 1.0 Ga mafic dykes and volcanic rocks in the Huili area, SW China: origin and tectonic significance. Precambrian Res 273:67–89. https://doi.org/10.1016/j.precamres.2015.12.011

Zhu Y, Lai SC, Qin JF, Zhu RZ, Zhang FY, Zhang ZZ, Gan BP (2019) Petrogenesis and geodynamic implications of Neoproterozoic gabbro-diorites, adakitic granites, and A-type granites in the southwestern margin of the Yangtze Block, South China. J Asian Earth Sci 183:103977. https://doi.org/10.1016/j.jseaes.2019.103977

Zhu Y, Lai SC, Qin JF, Zhu RZ, Zhang FY, Zhang ZZ (2020) Petrogenesis and geochemical diversity of Late Mesoproterozoic S-type granites in the western Yangtze Block, South China: co-entrainment of peritectic selective phases and accessory minerals. Lithos 352:105326. https://doi.org/10.1016/j.lithos.2019.105326

Zhu Y, Lai SC, Qin JF, Zhu RZ, Liu M, Zhang FY, Zhang ZZ, Yang H (2021) Neoproterozoic metasomatized mantle beneath the western Yangtze Block, South China: evidence from whole-rock geochemistry and zircon U-Pb-Hf isotopes of mafic rocks. J Asian Earth Sci 206:104616. https://doi.org/10.1016/j.jseaes.2020.104616